IEEE Access
Multidisciplinary | Rapid Review | Open Access Journal

Received September 6, 2019, accepted September 26, 2019, date of publication October 1, 2019, date of current version October 16, 2019.

Digital Object Identifier 10.1109/ACCESS.2019.2944794

Varying Speed Rate Controller for Human–Robot Teleoperation Based on Muscle Electrical Signals

XUE ZHAO, XIAOAN CHEN, YE HE, HONGLI CAO, AND TIANCHI CHEN
State Key Laboratory of Mechanical Transmission, Chongqing University, Chongqing 400044, China

Corresponding author: Ye He (hifish2@gmail.com)

This work was supported in part by the National Key Research and Development Program of China under Grant 2017YFB1301401, in part by the Graduate Scientific Research and Innovation of Chongqing, China, under Grant CYB19062, and in part by the Colleagues in SKLMT of Chongqing University.

ABSTRACT With the emergence of industrial robots in recent decades, advancing the technology that drives human-robot interaction has become a research hotspot. However, the control of human-robot interaction using human gestures has presented some challenges when applied to the industrial environment. For example, when a robot is controlled with a hand motion, the hand movement space may be smaller than the robot's working space, making it difficult to meet the robot's space and accuracy requirements. The research herein was centered on building interactive scenarios through unit software, and gesture recognition sensors were used to collect spatial information about the hand. A position mapping algorithm was used to map the position of the hand to the robot end-effector and a virtual robot space constraint was added to collectively allow users to control the robot's movements. In the experiment, volunteers were asked to control the robot by using constant speed ratio (Ratio of robot speed to input value) or changing speed ratio. The speed ratio affected the stability of the experiment, adding electromyography can improve the stability. The first innovation was the use of human muscle information as input information, adding it to the interaction based on unity. The second innovation was using an algorithm to change the mapping speed ratio according to the electromyography information provided. This was the first time that electromyography was used to change the mapping speed ratio of human-robot interactions, which may enable further advancements in human-robot interaction.

INDEX TERMS Human-robot interaction, tele-robot, virtual reality, EMG.

I. INTRODUCTION

Since the invention of the robot, humans have been working to improve the efficiency and safety of robot production, reduce the cost of robots, and simplify the operation process. Current robots are quite structurally mature, which can be seen in the robots used by companies such as ABB, Fanuc, and KUKA [1]. The robots most commonly used in the industry are reprogrammable robots, however, programming a robot for a specific task requires a lot of time and effort [2]. Although intelligent robots are able to fulfill human requirements and can autonomously adapt to changing environments, but they are subject to real-time conditions, and cutting-edge technologies such as sensor technology, image recognition technology, deep learning technology, and that full intelligent robots have not been implemented.

The associate editor coordinating the review of this manuscript and approving it for publication was Derek Abbott.

Applying human flexibility to a machine can allow for the accomplishment of many complicated tasks. Sheridan [3] proposed the concept of the tele-robot, which uses remote operation to extend a person's perception and manipulation capabilities to a remote location. Current teleoperation robots are used in many fields, such as the m2 model machine [4] that was used for isolating nuclear waste and tele-robots for nuclear power patrol [5]. Capocci [6] advanced a H300 MKII remote control robot that can be tested underwater at 300 meters. Ballantyne and Moll [7] looked at Intuitive's da Vinci surgical system, which combines teleoperation with medical care. In the field of micro teleoperation, Chinn *et al.* [8] designed a four-degrees-of-freedom AMTI telerobot which can be used to grasp and release micro-gear.

However, the above operations are based on remote sensing of the controller, etc., without using the human body's natural gesture language, which conforms with human habits. Authors in [9]–[11] used the human body's natural gestures to control the robot, but were limited by operational space

constraints (For a human may require less space for gestures than the robot needs to carry out its activities). Here is an example of spatial constraints: The active space of the hand is 1 and the active space of the robot is 3, we can set the attitude of the robot mapping coefficient to 3 to meet the robot's functional requirements. However, carrying out human gestures is not possible in all locations. If the mapping coefficient is increased to 6, part of the attitude movement can control the entire robot space, but the excessively large coefficient may cause jitter and reduce the accuracy of the control trajectory. Grafakos *et al.* [12] employed a human muscle electrical signal to change the stiffness of the dragging robot in order to study the influence on the robot's space drag. Wang *et al.* [13] integrated force control and electromyography (EMG) to enhance the performance of a tele-robot.

The problems encountered in previous studies is as follows. Using buttons to control the robot has many input dimensions and is not constrained by space, but it is difficult to operate. Using body language to control the robot's interaction conforms to the human body's own motion habits and has great potential, but it is restricted by space, so its practical application is limited.

A. CONSTRIBUTION

This study introduced a new dimension to solve the spatial constraints of natural limb control without changing the user's posture. Since the EMG signal can influence the space drag and impedance, we decided to apply EMG to teleoperation robots, to solve the space constraints problems. In the method, we use envelope, threshold and other technologies to process the collected EMG data, and the processed information was used to change the control of the robot. In terms of interaction accuracy and efficiency, the traditional body language interaction method is compared with the interaction method mentioned in this study in the virtual scene. It can found that the method of adding EMG dimension to change the interaction speed ratio mentioned in this paper is effective to solve the above spatial constraints.

B. OUTLINE

The paper consists of five Sections. In Section II, the system structure, data acquisition and processing methods are introduced. Then it introduces how to control the robot's movement, and how to apply EMG information to the formula to change the speed ratio of the robot's movement, and how to control the robot's rotation. The space constraints of robots and the experimental scenarios built in this study are also introduced. In Section III, we show the experimental results, mainly including the experimental time and accuracy data. In Section IV, the experimental results are analyzed in detail and explained. Conclusions are presented in Section V.

II. EXPERIMENTAL SETUP

A. SYSTEM STRUCTURE

The system structure of this study is shown in FIGURE 1. The user controls the movement of the robot inside the computer

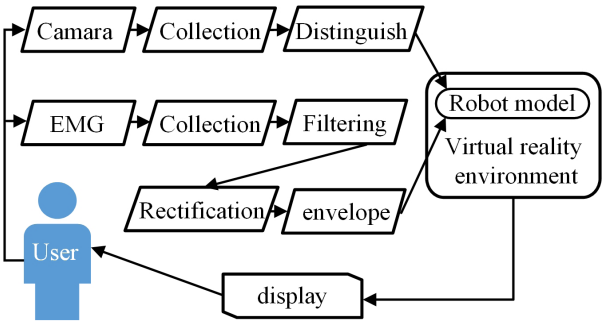

FIGURE 1. The camera collects the human hand posture and the muscle electricity sensor collects the arm tension. The hand controls the trajectory of the robot, and the muscle tension changes the control speed rate.

by hand. The position and posture of the human hand are recognized by a camera (Leap Motion sensor) arranged inside the space, and the degree of tightness of the human arm is recognized by the EMG sensor. The position, posture, and tightness are transmitted as a numerical signal to the robot model of the computer to control the operation of the robot end-effector. Kinematic modeling of robots is a relatively mature discipline, like Spong and Vidyasagar providing a kinematics model and inverse kinematics model method for robots [14], which could be used here.

B. MUSCLE ELECTRICAL SIGNAL

Before using the EMG information, it is useful to understand how the generation, collection, and processing of muscle electrical signals work. FIGURE 2 shows the muscle structure of a mammalian, composed of bundled muscle cells or fibers in the resting muscle, and maintaining a negative potential difference (−80 mV) through the myocyte membrane. When the nerve activates the fiber at the motor endplate, a reverse pulse potential (+30 mV) is formed for about 2 ms and this potential moves along the length of the fiber at a speed of 2-6 m/s. A potential difference is formed by arranging two electrodes (d+ and d−) at the position where the muscle fibers pass [15]. The muscle electrical signal is attenuated after passing through the subcutaneous tissue to the epidermis, and muscle tension signals are less than 1 mV. To obtain high-quality measurement signals and reduce interference, a differential amplifier is needed [9]. Hoffer and Perry [16] used 40-1000 Hz with an overall gain of 1000 as the EMG system bandwidth. The EMG (ZTEMG-1000) used in this study has a bandwidth of 10-1000 HZ with a gain of 1000, outputs the raw voltage signal. It's contact part is silver, which has good conductivity and has the advantage of reuse compared with wet EMG. Last Arduino was used to collect data, and the sampling rate was 500 HZ, then transfer the result to the virtual scene through serial port. A muscle electrical sensor was placement to measure forearm flexor like Fig. 3 A. In Fig. 3 B, the original signal collected is shown with the blue line, but the original signal is not used for direct control, as further processing of the signal is required. The process of signal processing is as follows (Fig. 3 B, C, and D).

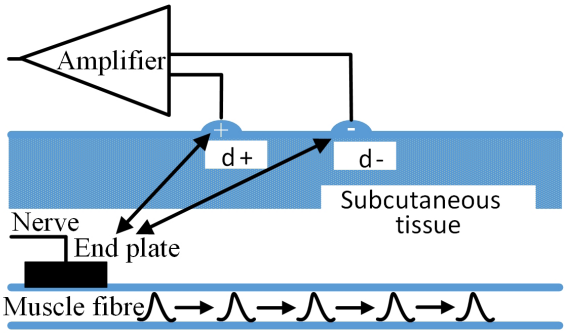

FIGURE 2. EMG signal transmission in muscle fibers.

Firstly, a 10-Hz-high-pass filter is used to suppress interference from the low-frequency signal (If the amplifier without bandwidth filter or high-pass filter, the process is needed). Due to the intensely positive and negative jumps in the signal, a modulus was given to shift the negative value to a positive direction through half-wave rectification. The amplitude information can be obtained by using the envelope filter, but it still has many peaks. The envelope signal is smoothed by 5 HZ, and the processed signal is shown with a red line. From the red line in FIGURE 3 D, it can be seen that tightening the muscles leads to an increase in the amplitude, which is the control parameter of the robot. It can be seen from the red line that there are four short arm muscles activated in the collection process, so there are four groups of peaks. When the arm muscles relax, the signal tends to be gentle (at $+0.05$ mv to -0.05 mv fluctuations). When the muscles are in a relaxed state, it can be seen that human control of muscle activation or relaxation is measurable. Due to individual differences, and in order to ensure control, this study used a normalized value (using the individual's maximum voltage as a divisor). Let ξ be the amplitude of the red envelope to indicate muscle activation ($\xi = U/U_{Max}$), then $\xi \in (0.1)$.

C. MANUAL POSITION OF ROBOT POSITION MAPPING

To control the robot using body language, it is necessary to clarify the kinematic relationship between the human body posture and the robot, and it is necessary to establish a kinematic model and transmit the human body posture to the robot through the model. The hand coordinates and the coordinates of the robot end-effector are shown in FIGURE 4. Because they are not in the same coordinate system, coordinate transformation is required. Where P denotes the coordinate system, {r} denotes the robot's coordinates, {h} denotes the hand coordinates, R denotes rotate, superscript r of P denotes the robot coordinate system, superscript h of P denotes the human hand coordinate system, U is the moving speed, and subscript n of P denotes a time series. The ratio of robot coordinates to human coordinates is a spatial transformation of constant, which can be expressed by formula (2). However, as the robot coordinates and the human body coordinate ratio are not constant, formula (2) cannot be directly solved. Traditionally, the mapping speed ratio of interactions

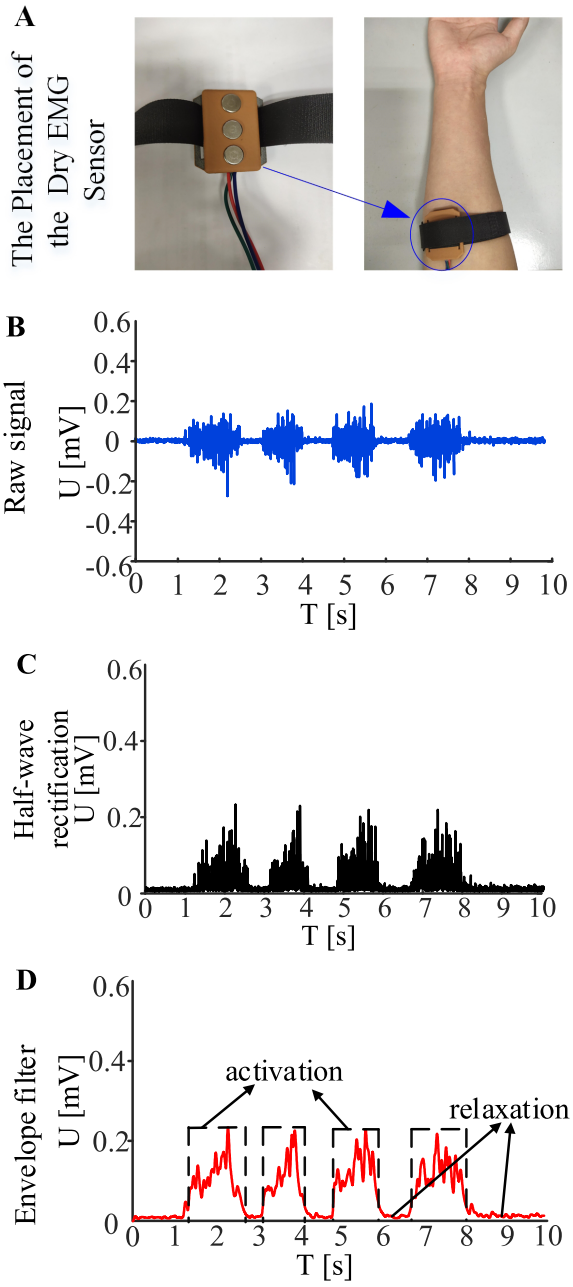

FIGURE 3. EMG indicates a state of activation or relaxation.

is always constant ($Const = V_{robot}/V_{input}$). This article adds the mapping parameter β which is the control coefficient for EMG. Adding the ratio of the hand movement space range to the robot movement space range, we get two constant ratios: $\beta = 2.5$ and $\beta = 5$. When $\beta = 2.5$, there is sufficient hand space to fully map the robot workspace, but only a portion of the hand space can map the whole robot workspace when $\beta = 5$. With the activation of the EMG signal, the variable mapping speed control expressed by formula (1). In theory, the threshold of signal can be simply chosen as 0.5, less than 0.5 means relaxation and more than or equal to 0.5 means tension. But from the actual point of view, it is appropriate for users to keep relaxed or semi-tightened all the time, but It is

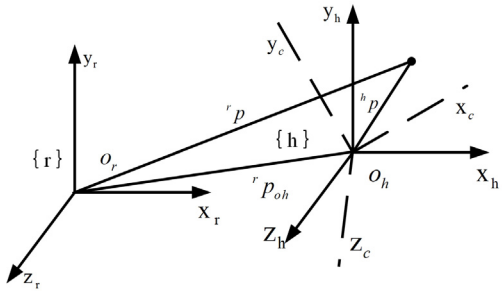

FIGURE 4. The coordinates of the hand in relation to the robot coordinates.

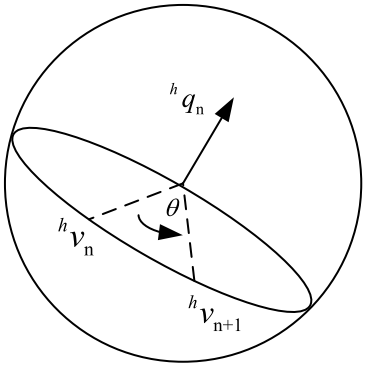

FIGURE 5. Rotation transformation of vectors by a quaternion.

not appropriate for users to keep maximum-tightened all the time. If users do not fully tighten and keep at 0.5 or so, it will lead to frequent state changes (stability will become worse). What we want is to increase the cost of switching (increase stability), but it's easier to maintain. So after practical experience, we choose two values 0.4 and 0.6 as thresholds, less than 0.4 as relaxation, more than 0.6 as tension, and 0.4 to 0.6 keep the previous state. When $\xi \leq 0.4$, the muscle is in a relaxed state, the state of the user's shape is drawn, and the speed ratio $\beta = 2.5$.let β keep the previous number when $0.4 < \xi < 0.6$. When $0.6 \leq \xi$ the muscles are in an active state and the speed ratio $\beta = 5$.

$$\beta = \begin{cases} 2.5, & \xi \leq 0.4 \\ \beta, & 0.4 < \xi < 0.6 \\ 5, & 0.6 \leq \xi \end{cases} \tag{1}$$

If the position and angle of the hand at the beginning and end of a single step has obtained. The velocity of the hand is multiplied by β and then transformed into the speed of the machine. Finally, the position of the robot is updated according to the position of the robot at the last moment. Using formulas (3), (4) and (5), the position of the robot can be calculated from the position of the hand.

$$^{r}\boldsymbol{P} = {}^{r}_{h}\boldsymbol{R}\,{}^{r}\boldsymbol{P}_{(n)} + {}^{r}\boldsymbol{P}_{oh} \tag{2}$$
$$^{r}\boldsymbol{P}_{(n+1)} = {}^{r}\boldsymbol{P}_{(n)} + \Delta t\,{}^{r}\boldsymbol{U}_{(n+1)} \tag{3}$$
$$^{r}\boldsymbol{U}_{(n+1)} = {}^{h}\boldsymbol{U}_{(n+1)}\beta \tag{4}$$
$$^{h}\boldsymbol{U}_{(n+1)} = ({}^{h}\boldsymbol{P}_{(n+1)} - {}^{h}\boldsymbol{P}_{(n)})/\Delta t \tag{5}$$

There are many well-developed methods that can be used to solve the problem of object rotation, such as Euler angles, rotation matrices, axis-angles, and quaternions. Yaw, pitch, and roll in the Euler angle are easy to understand, but there are Gimbal Lock problems [17], which can lead to angle mutation. The rotation matrix has no Gimbal Lock problem, but it is not intuitive and wastes memory as it requires nine parameters to represent three-degrees-of-freedom rotation. Axis angle rotation is not intuitive without the Gimbal Lock problem, but it is difficult to implement multiple rotation combinations, and it is not easy to linearly interpolate its elements. The quaternion has no Gimbal Lock problem and only four numbers are used in order to prevent memory waste, making it easy to use. Formula (19) is the renewal formula of the robot rotation. The specific idea is to obtain the rotation axis and rotation angle of the human hand, and then update the rotation state of the robot. Formula (6) to Formula (18) is a concrete deduction process. The quaternion consists of a scalar and a vector, assuming that the three-unit vectors of the standard orthogonal basis in the three-dimensional space are $\hat{i} = (1, 0, 0)$, $\hat{j} = (0, 1, 0)$ and $\hat{k} = (0, 0, 1)$, and the quaternion can be expressed by formula (6). Another way to represent quaternions like formula (7) is where θ indicates the angle of rotation around the axis of rotation and $\hat{\mathbf{u}} = (\hat{i}, \hat{j}, \hat{k})$, which indicates the axis of rotation. The unit quaternion, where $|q| = q_0^2 + \|q\| = 1$, can be calculated by formula (8).

$$q = q_0 + \mathbf{q} = q_0 + q_1\hat{i} + q_2\hat{j} + q_3\hat{k} \tag{6}$$
$$q = \cos\frac{\theta}{2} + \hat{\mathbf{u}}\sin\frac{\theta}{2} \tag{7}$$
$$\hat{\mathbf{u}} = q/\|q\| \tag{8}$$

As per FIGURE 5, set ${}^{h}q_{(n)}$ as the unit quaternion of the hand, let ${}^{r}q_{(n)}$ be the unit quaternion for the end of the robot, ${}^{h}v_n$ represents the vector of the hand, $v \in \Re^3$.${}^{h}q_{(n)}$ is the variation of ${}^{h}q$ in the time series n, and the vector rotation quaternion sequence is expressed as formula (9).

$${}^{h}v_{n+1} = L_{{}^{h}q_{(n+1)}}({}^{h}v_0) = L_{\Delta^{h}q_{(n+1)}\Delta^{h}q_{(n)}\ldots{}^{h}q_{(0)}}({}^{h}v_0) \tag{9}$$

To map the rotation of the hand to the end of the robot, the rotation axis and rotation angle of the hand must be obtained, which can be done by changing quaternion $\Delta^{h}q_{(n+1)}$ as per formula (10).

$${}^{h}q_{(n+1)} = \Delta^{h}q_{(n+1)}\,{}^{h}q_{(n)} \tag{10}$$
$$\Delta^{h}q_{(n+1)} = {}^{h}q_{(n+1)}\,{}^{h}q^{-1}_{(n)} \tag{11}$$

For a unit quaternion, its inverse is equal to its conjugate, as per formula (12). ${}^{h}q^{*}_{(n)}$ as per formula (13).

$${}^{h}q^{-1}_{(n)} = {}^{h}q^{*}_{(n)} \tag{12}$$
$${}^{h}q^{*}_{(n)} = {}^{h}q_{(n)0} - {}^{h}q_{(n)1}i - {}^{h}q_{(n)2}j - {}^{h}q_{(n)3}k \tag{13}$$

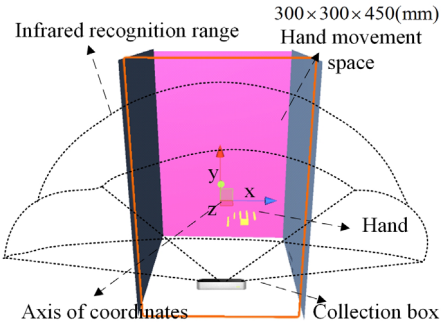

FIGURE 6. The movement of the hand.

The solution of $\Delta^h q_{(n+1)}$ in formula (11) is not a unit quaternion, which needs to be converted into a unit quaternion like formula (14).

$$\Delta^h q_{(n+1)} \leftarrow \Delta^h q_{(n+1)} \Big/ \left\| \Delta^h q_{(n+1)} \right\| \tag{14}$$

The change of rotation angle and axis of the hand can be obtained by formulas (15) and (16).

$$\Delta^{\mathrm{h}}\theta_{(n+1)} = 2\arccos(\Delta^h \mathrm{q}_{(\mathrm{n+1})0}) \tag{15}$$

$$\hat{\mathbf{u}} = [\Delta^h q_{(n+1)1}, \Delta^h q_{(n+1)2}, \Delta^h q_{(n+1)3}]^T \Big/ \sin\frac{\Delta^h \theta_{n+1}}{2} \tag{16}$$

The rotation angle and the rotation axis of the hand change are the same as that of the robot, and the rotation map is as shown in formula (17), where $\Delta^r\theta_{(n+1)}$ is the angle change of the end of the robot in n +1 sequence. The quaternion of the end of the robot in the n + 1 sequence is shown in formula (19).

$$\Delta^{\mathrm{r}} q_{(n+1)} = (\cos\frac{\Delta^r\theta_{(n+1)}}{2}, \hat{\mathbf{u}}\sin\frac{\Delta^r\theta_{(n+1)}}{2}) \tag{17}$$

$$\Delta^r\theta_{(n+1)} = \Delta^h\theta_{(n+1)} \tag{18}$$

$${}^{\mathrm{r}}q_{(n+1)} = \Delta^{\mathrm{r}} q_{(n+1)}\,{}^{\mathrm{r}}q_{(n)} \tag{19}$$

D. EXPERIMENTAL EQUIPMENT AND WORKING CONDITIONS

For direct access to hand data, this research used the Leap Motion device. Infrared LED illuminates the area above the controller. Two cameras capture the hand image and calculate the relative position of the hand in space by a triangulation algorithm. Leap Motion provides coordinates, speed, and the normal direction of the palm. It's recognition ranges from 25 mm to 600 mm above the top of the controller, just like an inverted quadrangular pyramid. The moving area of the hand is shown in FIGURE. 6, where the moving space of the hand is $300mm \times 300mm \times 400mm$. Leap Motion recognizes the motion of the finger with a theoretical recognition accuracy of 0.01 mm and a recognition delay of 5-10 ms. It's SDK provides APIs for multiple languages such as C++, C#, Java, JavaScript, and Python. In the scene operation, unity can render the scene and provide for a basic physics engine, such as friction, gravity, and torque, and establish

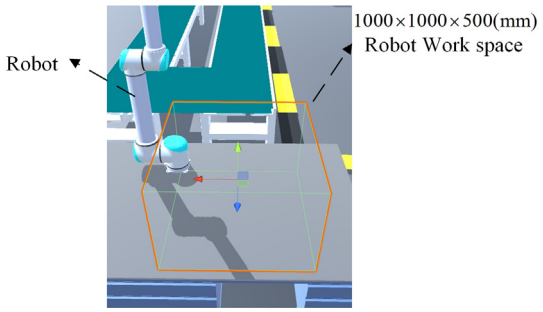

FIGURE 7. The operation space of the robot.

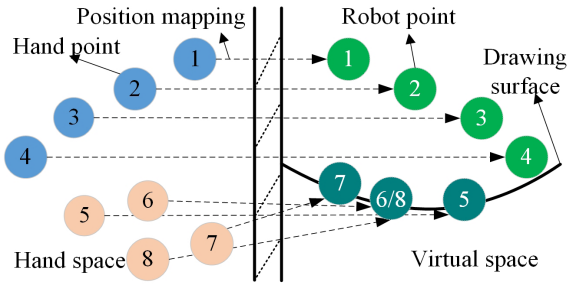

FIGURE 8. Human-robot position mapping relationship.

various object connection relationships, such as providing hinges, spring connections, etc. The robot running space is shown in FIGURE 7, where the yellow rectangle is the robot workspace, and the length, width height are $1000mm \times 1000mm \times 500mm$. It is easy to set up experimental scenes for C# supported by Leap motion and unity, and this set up can allow for the use of a high number of library functions. In addition to mathematical operations, it also provides various IO ports and can output model data to other software in real-time via UDP or TCP, or read other software in real-time. Experimental data can also be saved to a computer in the form of text. The experiments were run on a PC with an Intel Core i7-8700 CPU @3.20GHz, and 16GB of RAM, connected to a 27-inch LED with 1920 × 1080 resolution at 60 Hz, running on Windows 10.

This experiment requires paint curves on a surface of the plane. In the real world, with force control, a distance sensor or human observation can be used to keep the end of the robot in a specific plane. However, in virtual interactions without force feedback, it is very difficult for the participant to control the end of the robot on a specific curved surface. In this study, the position of the robot end is constrained by the following method. In FIGURE 8, when the end position of the robot is above the drawing surface, the hand position to the robot position map uses formula (3), and the mapping is represented by circles 1 to 4. When the robot touches the drawing surface, if the hand moves continuously down, the robot will not move along the normal direction of the drawing surface. When the hand moves in a horizontal direction, the robot will only follow formula (3) along the tangential direction of the surface, but deep mapping is represented by circles 5 to 8. By using

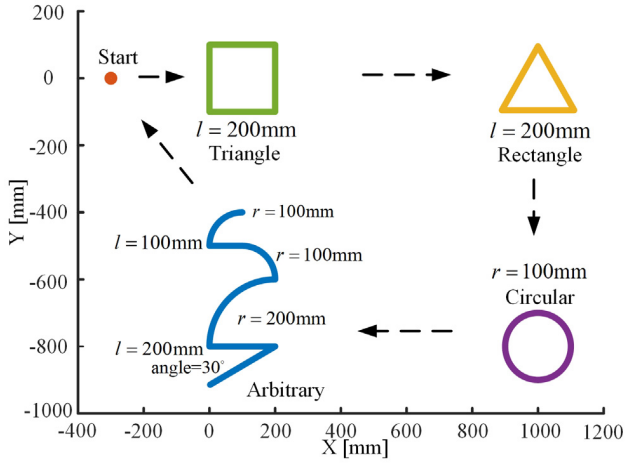

FIGURE 9. The target curves.

the above method, there is no displacement restriction on the user's motion, while the end of the robot can be kept on a specific curved surface. In addition, when designing the virtual interaction structure, it should be noted that the user tends to ignore the depth when the hand is down, causing the robot to leave the surface too long after the hand is raised. Therefore, a layer of luminescent substance was wrapped around the end of the robot, which will display different lengths according to the depth, reminding the user of the current depth.

Curves may change according to the varying shape of the work-piece in most situations. Although they are highly unstable structures, they are also composed of basic curves, such as horizontal, vertical, oblique, arcs, and arbitrary polygonal lines. The entire trajectory of this study design is shown in FIGURE 9. The participator needs to control the robot start from point A, draw a rectangle according to the dotted arrow, then draw a triangle, circle, multiple curved lines, and finally return to point A. The points of interest we focus on include the following: interaction time and drawing quality.

The experiment was divided into three groups: A, B, and C. Four healthy male volunteers had a mean age of 26±2.4 years (range 24-27 years), a mean mass of 66.16 kg (± 4.67 kg), and a mean weight of 1.75m (± 0.04 m) participated in the experiment, they are all students in mechanical specialty of Chongqing university. Each person participated in every group and repeated the exercise twice. Groups A and B did not wear EMG equipment, the velocity ratio of group A was $\beta = 2.5$, the B group velocity ratio was $\beta = 5$, while group C wore EMG equipment and their velocity ratio β was based on formula (1). Before the experiment, each participant will have 5-10 minutes for video introduction and question answering, and then will be familiar with the operation, each operation will be familiar with 5-7 minutes. After the experiment started, the experiment was started in the order of ABC and then CBA, and each group gap would rest for 2-3 minutes.

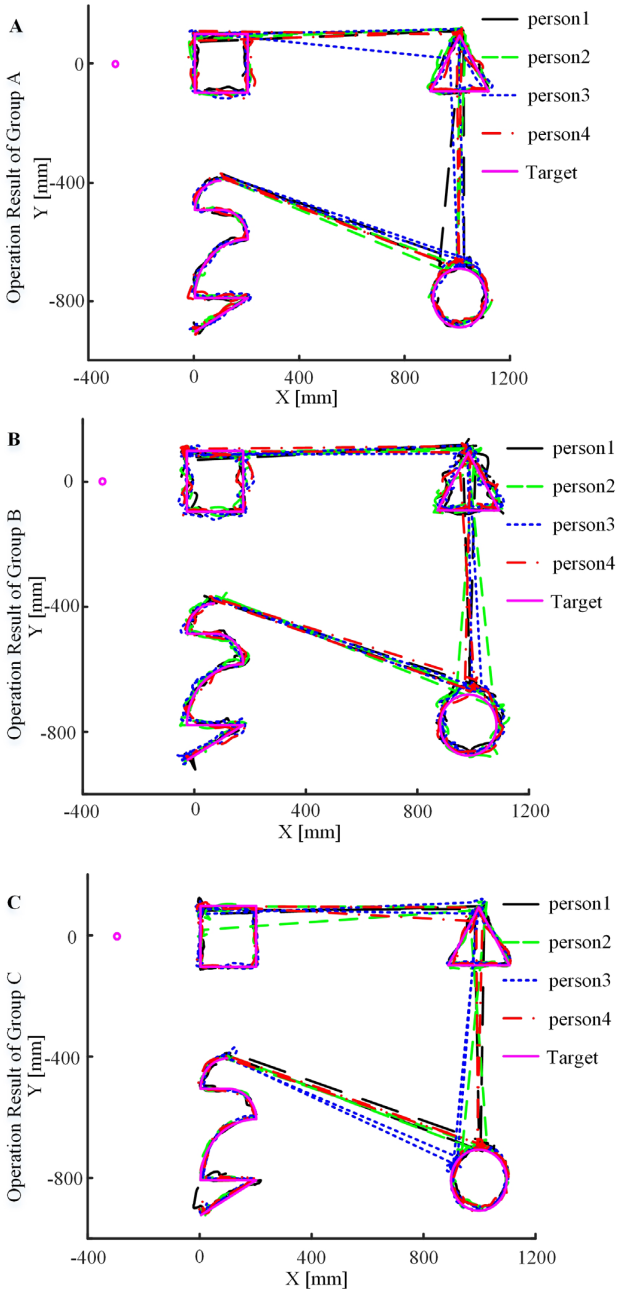

FIGURE 10. Curve drawing at the end of the robot.

III. RESULT

A. DRAWING REULTS

In order to study the influence of different mapping speed ratios β on efficiency and accuracy, the experimental results of groups A, B, and C are shown in FIGURE 10. Since each group drew the shapes two times, each group produced eight curves. It can be seen that the A, B, and C groups drew all curves according to the requirements.

B. INTERACTION TIME

FIGURE 11 shows the drawing situation of a person. The data was marked by stages (n = 0 to 8). t1, t3, t5, and t7

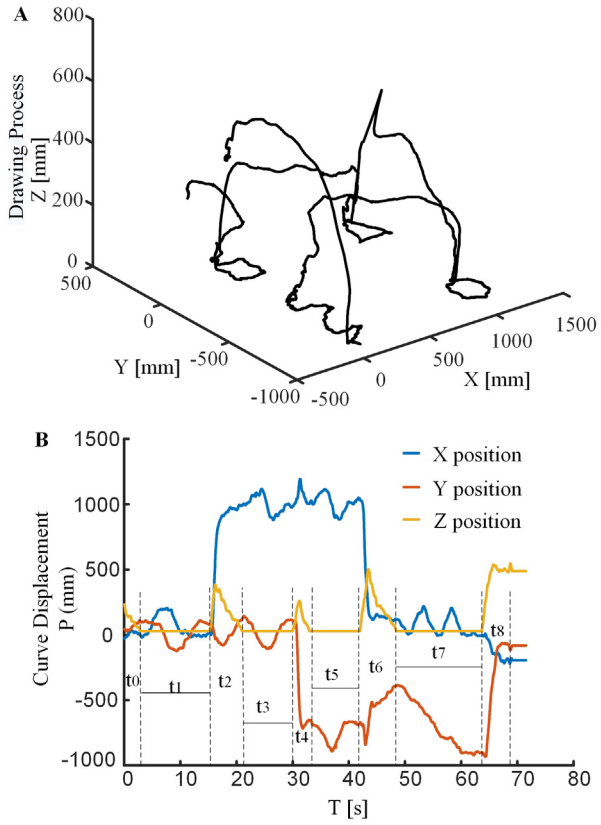

FIGURE 11. Drawing process and time taken at different stages of the experiment. A is the drawn curve. B is the XYZ displacement of the drawn curve.

represent the time taken to draw a triangle, rectangle, circle, and arbitrary polygon, while t0, t2, t4, t6, and t8 is the time taken to move from one graph to another.

In order to study the different times taken between the different groups, all the data is displayed in a box diagram, as shown in Table 1, where T is the time taken to draw the rectangle, R is the time taken to draw a triangle, A is the time taken to draw the arbitrary polygon, C is the time to draw a circle, and M is the time taken to complete the whole movement, which equals the sum of t0, t2, t4, t6, and t8. Sum1 represents the total time spent drawing, equal to the sum of T, R, A, and C. SUM2 represents the time taken to complete the sum of M and SUM1. The total times taken are shown in FIGURE 12. From SUM1, group A took an

average time of 48.76 s, group B took an average time of 45.48 s, and group C took an average time of 65.77 s. A repeated measure multi-way analysis of variance by SPASS showed that there were significant differences ($p = 0.002$) in the time taken among group A, group B, and group C. Group A and group B had no significant differences ($p = 0.495$) but both fast than group C ($p < 0.05$). The differences among participants was not significant ($p = 0.453$). That is to say, the change in constant β between the two groups did not significantly influence the time taken, contrary adding EMG change β did increased time taken. Looking

TABLE 1. The times taken to complete the experiment testify to its stability.

Person	Curve	TIME times1 Group A	times1 Group B	times1 Group C	times2 Group A	times2 Group B	times2 Group C
	T	12.35	6.90	17.24	10.48	11.98	12.38
	R	9.86	7.00	16.82	10.46	8.46	14.95
	A	14.70	16.39	18.76	11.56	15.21	21.91
1.00	C	12.25	10.51	12.74	18.47	8.38	13.36
	M	29.80	27.65	29.64	25.19	25.06	22.37
	SUM1	49.15	40.79	68.95	50.97	44.03	62.59
	SUM2	78.95	68.44	98.59	76.16	69.09	84.96
	T	11.89	10.08	11.15	8.37	9.18	19.26
	R	9.04	6.71	15.01	8.16	9.35	17.79
	A	19.90	15.90	21.10	17.78	18.17	19.69
2.00	C	12.74	9.50	12.03	11.19	8.17	18.51
	M	21.97	29.90	25.92	22.47	25.73	23.02
	SUM1	53.58	42.19	59.30	45.50	44.88	75.26
	SUM2	75.55	72.09	85.22	67.97	70.61	98.28
	T	10.65	13.65	13.79	7.59	7.51	12.88
	R	7.29	12.00	14.05	7.44	10.14	12.03
	A	13.64	16.70	20.71	16.72	12.73	18.51
3.00	C	7.86	12.20	19.69	8.47	7.46	15.72
	M	23.91	29.76	25.99	22.72	25.08	26.02
	SUM1	39.43	54.55	63.41	40.22	37.84	59.14
	SUM2	63.35	84.31	89.40	62.93	62.91	85.16
	T	10.97	11.69	10.48	7.67	8.87	8.57
	R	9.37	8.82	11.25	7.56	6.73	15.53
	A	15.30	11.79	19.11	16.70	14.26	13.28
4.00	C	11.87	8.77	13.55	8.71	6.96	15.53
	M	26.14	24.07	30.04	23.28	21.68	30.22
	SUM1	47.34	41.07	54.40	40.64	36.82	52.91
	SUM2	73.65	65.14	84.44	63.92	58.51	83.13

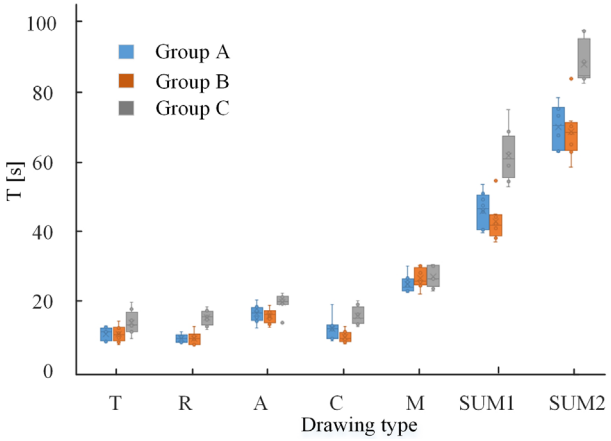

FIGURE 12. Comparison of time spent on the experiment by the groups.

at M from groups A, B, and C, no significant differences were found ($p = 0.440$) for each group. There were not significant differences among participants ($p = 0.210$). For SUM2, group A took an average time of 70.31 s, group B took an average time of 68.89 s, and group C took an average time of 89.40 s. Significant differences between group A, group B and group C ($p < 0.05$). There were no significant differences ($p = 0.673$) found in time between group A and group B but both fast than group C ($p < 0.05$). The differences among participants were not significant ($p = 0.202$). It can be seen that groups A and B are close, with both producing lower values than group C. From the whole experiment, it can be seen that increasing β does not significantly reduce the time

TABLE 2. The sd values 0btained support the stability of the experiment.

Person	Curve	SD times1 Group A	times1 Group B	times1 Group C	times2 Group A	times2 Group B	times2 Group C
1.00	T	8.66	9.65	6.69	5.21	9.67	4.83
	R	7.48	14.88	5.95	7.94	17.82	7.81
	A	6.51	8.44	6.76	7.49	8.32	8.66
	C	11.63	18.91	13.32	12.24	18.39	11.56
	total	8.36	12.33	8.08	7.90	12.40	8.31
2.00	T	4.48	8.75	6.08	5.45	8.11	4.05
	R	11.65	12.18	7.64	11.50	10.90	6.52
	A	5.65	7.94	6.03	5.28	9.62	4.78
	C	14.49	19.79	8.08	14.03	14.72	10.65
	total	8.51	11.38	6.96	8.58	10.51	6.37
3.00	T	8.11	8.67	6.45	4.73	10.22	3.52
	R	6.63	9.69	6.18	9.01	14.00	6.27
	A	7.49	9.02	6.22	6.07	10.89	8.61
	C	13.84	18.75	7.12	10.71	16.18	7.25
	total	9.01	11.19	6.48	7.32	12.63	6.65
4.00	T	7.48	9.33	5.91	6.76	10.75	3.42
	R	7.34	13.26	7.25	9.31	5.94	6.15
	A	6.55	7.34	6.79	7.30	7.51	6.47
	C	12.81	13.38	8.93	13.15	12.70	10.98
	total	8.49	10.47	7.25	8.91	8.85	7.09

taken to complete the experiment, while adding EMG did not change the movement time but did increase the interaction time. By observing the whole experiment process, the time increase caused by adding EMG may be due to participants' active control of state switching and distraction. A more detailed explanation is that there is no significant difference between Group A, B and C in the moving phase for there is no need to pay attention to the accuracy of the curve. In the process of drawing, group A and B only needs to pay attention to the accuracy of the curve, but for group C whom need to pay attention to both the requirements of the curve and muscle tightness, which may lead to distraction and unconscious slowdown of the speed. However, this speed effect is still acceptable in practical application. After all, many applications require higher accuracy, such as teleoperation control bomb disassembly, relative to increasing time.

C. DRAWING STABILITY

The data used in this experiment include two-dimensional coordinate positions. To study the differences in stability between the different groups, the data needs to be further processed. By calculating the distance between the actual coordinate and the target coordinate, therefore making it one-dimensional, then using the distance standard deviation (SD) to evaluate the stability of the experiment, we find that the smaller the SD value, the closer the actual coordinate is to the target position, and the more stable the rendering is. As shown in formula (20), where x, y are the actual drawing coordinates, x_{tc}, y_{tc} are the target coordinates with the smallest distance from x, y. After processing all the data, the results are shown in Table 2, where T, R, A, and C represent each drawing error, respectively, and together give the total process error for the whole drawing. For drawing T, group A, B and C had significance different ($p = 0.001$), group A and C was better than group B ($p < 0.05$), and group C was similar to group A ($p = 0.133$). For drawing R, group A, B and C had significance different ($p < 0.001$), group A and C was better than group B ($p < 0.05$), and group C was no significance different to group A ($p = 0.056$). For drawing A, group A, B and C had significance different ($p = 0.001$), group A and C was better than group B ($p < 0.05$), group C was similar to group A ($p = 0.607$). For drawing C, group A was better than group B ($p < 0.05$), and group C was better than group A ($p < 0.05$).

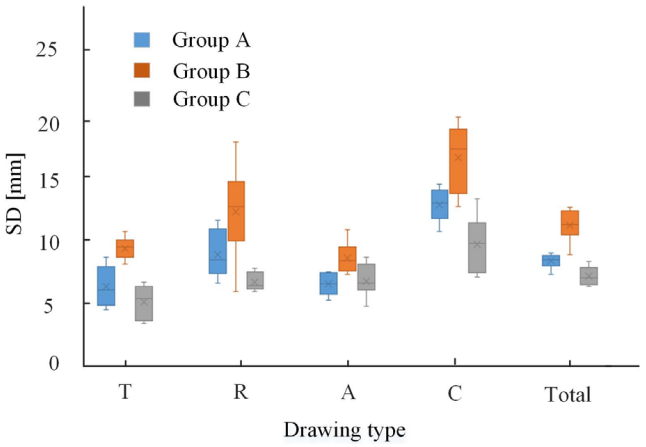

FIGURE 13. Comparison of SD values between the groups.

Overall, group A (8.37), B (11.22) and C (7.15) had significance difference ($p < 0.001$), group A was superior to group B ($p < 0.05$), and group C was superior to group A ($p < 0.05$). There were not significant differences among participants ($p = 0.059$). It can be seen that the smaller the value of β, the closer the graph is drawn to the target curve, the total situation is as FIGURE 13 group C has the best stability.

$$\mathrm{SD} = \sum \left\| X - \bar{X} \right\| \Big/ \mathrm{n} = \sum \|(x - x_{\mathrm{tc}}, y - y_{\mathrm{tc}})\| / \mathrm{n} \qquad (20)$$

IV. DISCUSSION

In this study, virtual reality technology was used to simulate the path calibration process of an operational telerobot, and the effects of conventional interaction and muscle electrical signal interaction on the operation were compared. This research is important because it opens up new possibilities to collect human bioelectrical information and use it in virtual reality interactions. As far as we know, this is the first time that muscle electrical signals have been applied to virtual reality in human-robot interactions while changing the mapping speed ratio of the virtual interactions. Our research differed from that of previously published articles, which instead focused on force feedback interaction. References [12], [18], [19] or network delay [20]. Examining the operating space is not enough. This study is based on using a small hand movement space to control the large operational space used by a robot, examining the

influence of different speed ratios β on the human-robot interaction.

In terms of the time taken to complete the interaction, we find that the mapping speed ratio did not significantly influence the operation time. Looking at the accuracy of the interaction, we find that the smaller the β, the better the stability. In this case, the mapping speed ratio needs to be reduced. In terms of space limitations and stability, we can use a smaller coefficient to ensure better control. The stability of group C was significantly higher than group A and group B. For group A, the constant $\beta = 2.5$ approaches the minimum boundary value. That is to say, adding the muscle electrical signal to dynamically change the β between 1 and 5 can solve the above problems. Of course, there are still some things that can be improved in this study, such as using a virtual reality helmet to further enhance reality. In this study, we studied the effects of EMG on virtual reality human-telerobot interaction, and improved the interaction quality by changing the interaction rate ratio through human arm EMG information. This study shows that virtual reality interaction is not only based on spatial or force interaction, but information from other human body variables can be incorporated to improve accuracy and control. It is advantageous to add EMG to VR or teleoperation. Because dimension is single in the traditional interactive input information, generally only attitude input. There are few ways to increase dimensionality, like force feedback, but it is huge and expensive. The method of use language adding dimension is feasible, and it is generally used in vehicle navigation, mobile phone interaction, etc., but it will affect the people nearby in VR entertainment or work. In this study, EMG is added, users can control the robot running in VR in two dimensions. In addition, button-controlled input, regardless of the nature of finger interaction, a button to control a dimension is feasible and commonly used. But for experience more realistically (through natural posture control), it is not appropriate to add control buttons to the scene, for users need to constantly change their current posture to touch the button. On the contrary EMG will not change the user's posture because the occupancy is due to muscle tightness.

V. CONCLUSION

With the development of virtual reality technology, human-robot interaction can be successfully operated in the virtual reality world. However, human-robot interaction in virtual reality is relatively fixed, resulting in conflicts between the interaction quality and space. The first innovation herein was to use human muscle information as input information and add it to the interaction based on unity. The second innovation was to determine how to map the position angle information of the hand to the end of the robot, formulating an algorithm to change the mapping speed ratio according to the electromyography information provided. From the experiment, we came to the conclusion that increasing the mapping coefficient did not save interaction time and reduced accuracy, as could be seen in group A and group B. Changing the mapping coefficient β in real-time by introducing electromyography information could ensure high accuracy in the same space. The human-robot interaction mapping method, incorporating electromyography, is expected to facilitate further advancements in the industry, with a particular emphasis on using human biological information to improve interaction.

REFERENCES

[1] C. Thomas, B. Matthias, and B. Kuhlenkötter, "Human-robot-collaboration-new applications in industrial robotics," in *Proc. Ind. Robot. Int. Conf. Competitive Manuf.*, 2016, pp. 293–299.

[2] Z. Pan, J. Polden, N. Larkin, S. V. Duin, and J. Norrish, "Recent progress on programming methods for industrial robots," in *Proc. ISR*, Jun. 2010, pp. 1–8.

[3] T. B. Sheridan, "Telerobotics," *Automatica*, vol. 25, no. 4, pp. 487–507, 1989.

[4] R. C. Goertz, *Mechanical Master-Slave Manipulator*, vol. 12. Nucleonics (US) Ceased Publication, 1954.

[5] J. S. Albus, "Trip report: Japanese progress in robotics for construction," *Robotics*, vol. 2, no. 2, pp. 103–112, 1986.

[6] R. Capocci, G. Dooly, E. Omerdić, J. Coleman, T. Newe, and D. Toal, "Inspection-class remotely operated vehicles—A review," *J. Mar. Sci. Eng.*, vol. 5, no. 1, p. 13, 2017.

[7] G. H. Ballantyne and F. Moll, "The da Vinci telerobotic surgical system: The virtual operative field and telepresence surgery," *Surg. Clin. North Amer.*, vol. 83, no. 6, pp. 1293–1304, 2003.

[8] D. Chinn, P. Ostendorp, M. Haugh, R. Kershmann, T. Kurfess, A. Claudet, and T. Tucker, "Three dimensional imaging of LIGA-made microcomponents," *J. Manuf. Sci. Eng.*, vol. 126, no. 4, pp. 813–821, 2004.

[9] M. Al-Mouhamed, O. Toker, A. Iqbal, and M. Nazeeruddin, "A distributed framework for relaying stereo vision for telerobotics," in *Proc. IEEE/ACS Int. Conf. Pervasive Services (ICPS)*, Jul. 2004, pp. 221–225.

[10] M. Becker, E. Kefalea, E. Maël, C. Von Der Malsburg, M. Pagel, J. Triesch, J. C. Vorbrüggen, R. P. Würtz, and S. Zadel, "GripSee: A gesture-controlled robot for object perception and manipulation," *Auton. Robots*, vol. 6, no. 2, pp. 203–221, 1999.

[11] H. Zhong, J. P. Wachs, and S. Y. Nof, "A collaborative telerobotics network framework with hand gesture interface and conflict prevention," *Int. J. Prod. Res.*, vol. 51, no. 15, pp. 4443–4463, 2013.

[12] S. Grafakos, F. Dimeas, and N. Aspragathos, "Variable admittance control in pHRI using EMG-based arm muscles co-activation," in *Proc. IEEE Int. Conf. Syst. Man Cybern. (SMC)*, Oct. 2016, pp. 001900–001905.

[13] N. Wang, C. Yang, M. R. Lyu, and Z. Li, "An EMG enhanced impedance and force control framework for telerobot operation in space," in *Proc. IEEE Aerosp. Conf.*, Mar. 2014, pp. 1–10.

[14] M. W. Spong and M. Vidyasagar, *Robot Dynamics and Control*. Hoboken, NJ, USA: Wiley, 2008.

[15] C. A. Tucker, *Measuring Walking: A Handbook of Clinical Gait Analysis*, vol. 26. Alexandria, VA, USA: Pediatric Physical Therapy (US), 2014.

[16] M. M. Hoffer and J. Perry, "Pathodynamics of gait alterations in cerebral palsy and the significance of kinetic electromyography in evaluating foot and ankle problems," *Foot Ankle Int.*, vol. 4, no. 3, pp. 128–134, 1983.

[17] D. Hoag, "Apollo guidance and navigation considerations of Apollo IMO gimbal lock," Massachusetts Inst. Technol., Cambridge, MA, USA, Tech. Rep. E-1344, 1963.

[18] H. Cao, X. Chen, Y. He, and X. Zhao, "Dynamic adaptive hybrid impedance control for dynamic contact force tracking in uncertain environments," *IEEE Access*, vol. 7, pp. 83162–83174, 2019.

[19] H. Cao, Y. He, X. Chen, and Z. Liu, "Control of adaptive switching in the sensing-executing mode used to mitigate collision in robot force control," *J. Dyn. Syst. Meas. Control*, vol. 141, no. 11, 2019, Art. no. 111003.

[20] P. Fraisse and A. Lelevé, "Teleoperation over IP network: Network delay regulation and adaptive control," *Auton. Robots*, vol. 15, no. 3, pp. 225–235, 2003.

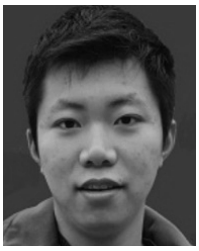

XUE ZHAO was born in Chongqing, China, in 1992. He is currently pursuing the Ph.D. degree in mechanical engineering with the State Key Laboratory of Mechanical Transmission, Chongqing University, Chongqing. His research interests include to study how to improve the efficiency and flexibility of production and assembly through human–robot cooperation, including sensor integration, human body information collection, data fusion, control strategy, innovation, and many other issues.

XIAOAN CHEN received the B.S. degree in mechanical engineering from Sichuan University, Chengdu, China, in 1982, the M.S. and Ph.D. degrees in mechanical engineering from Chongqing University, Chongqing, China, in 2000.

From 1996 to 2000, he was a Research Assistant with the State Key Laboratory of Mechanical Transmission. Since 2000, he has been a Professor with the Mechanical Engineering Department, Chongqing University. His research interests include high-speed motorized spindle, precision transmission and drive, and intelligent robot control.

Dr. Chen is the Editor-in-Chief of the *Journal of Modern Manufacturing Engineering*.He was a recipient of the Second Prize of the National Science and Technology Progress Award.

YE HE received the B.S. degree in mechanical engineering from Chongqing Technology University, Chongqing, China, in 2000, the M.S. degree in mechanical engineering from Chongqing University, Chongqing, in 2003, and the Ph.D. degree in mechanical engineering from the State Key Laboratory of Mechanical Transmission, Chongqing University, in 2019.

Since 2004, he has been a Research Assistant with the State Key Laboratory of Mechanical Transmission. His research interests include high-speed motorized spindle, automobile transmission, virtual digital manufacture, intelligent structure design and control, and human–robot collaborative.

HONGLI CAO was born in Xi'an, Shanxi, China, in 1992. He received the B.S. degree in mechanical design, manufacture, and automation and the M.S. degree in mechanical engineering from the University of Chongqing, Chongqing, China, in 2015. He is currently pursuing the Ph.D. degree in mechanical engineering with the State Key Laboratory of Mechanical Transmission, Chongqing University.

In 2016, he was a recipient of the Honor of Excellent Graduate Student of Chongqing University. His research interests include vibration control of high-speed motorized spindle, robot visual servo control, robot compliance control, and human–robot interaction.

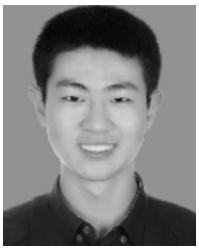

TIANCHI CHEN was born in Shandong, China, in 1995. He received the B.E. degree in mechanical engineering from the Qingdao University of Science and Technology, China, in 2017. He is currently pursuing the Ph.D. degree in vehicle engineering with the State Key Laboratory of Mechanical Transmission, Chongqing University. His research interests include physical human–robot interaction technologies, exoskeleton robot, sensor fusion, and signal processing.